JOURNAL OF OPTOELECTRONICS AND ADVANCED MATERIALS Vol. 10, No. 10, October 2008, p. 2653 - 2656

Spectroscopic investigation of porous silicon prepared by laser-induced etching

KHALID M. OMAR*, N. K. ALI, Z. HASSAN, M. R. HASHIM, H. ABU HASSAN
School of Physics, Universiti Sains Malaysia, 11800-Penang, Malaysia

Porous silicon was prepared by using an argon-ion laser in a laser-induced etching process with different etching time. Scanning electron microscopy was used to monitor changes in surface morphology produced during the etching process. Porous silicon samples were subjected to spectroscopic investigations. The first-order Raman line asymmetry was found to decrease with increase of the etching time, while the peak position downshifted for a given power density. The photoluminescence spectra (PL) exhibit a blue shift in peak position with etching time. Both Raman and PL data were explained using appropriate quantum confinement models involving three-dimensional confinement and Gaussian size distributions of nanocrystallites constituting porous silicon samples. There is reasonable agreement between the results obtained from Raman and PL spectroscopic investigations of the PS samples.

(Received May 14, 2008; accepted August 14, 2008)

Keywords: Porous silicon, Laser- induced etching, Raman spectra, Photoluminescence

1. Introduction

Porous silicon (PS) layers have been intensely studied since the discovery of an efficient visible luminescence in 1990 [1]. Light emitting silicon nanostructures have been produced by using a wide range of different techniques [2, 3]. Electrochemical anodization with direct current (dc) is the most commonly used technique for the formation of porous semiconductors [4-6]. Both the thickness and the crystallite size can be adjusted with this technique, thus enabling us to control the optical and electrical behavior of PS layers [7]. However, isolating the metal contacts from the solution has been the major drawback of this technique. Stain-etching technique (electroless) can also be used to form porous layers in Si [8]. Major difference between the two techniques is the formation rate and the thickness limitation in the latter one. Recently, a new method, termed metal-assisted chemical etching, has been developed, which is relatively simple compared to the anodization method. It needs no electrodes on the back surface of Si wafers and enables formation of uniform porous silicon layers [9,10].

Laser induced etching is another versatile technique that allows the formation of nanostructures which are determined by the photon energy, power density of laser beam illumination on the sample surface and the routine parameters like types of etchants, composition of electrolyte, temperature etc. Reports are available in the literature about this etching technique employed for Si [11, 12] and GaAs [13] nanostructures fabrication. In this work, we have fabricated PS nanostructure by laser-induced etching using an argon-ion laser (λ= 488 nm), which is probably the simplest technique to produce nanocrystallites and sizes can be controlled by changing the etching time. The information regarding the surface morphology can be obtained by using scanning electron microscopy (SEM). Photoluminescence and Raman spectroscopic studies are also reported to examine the formation of nanocrystallites in the PS after laser etching. The size and size distributions estimated by the analysis of the PL and Raman data using the existing quantum confinement models agree reasonably well.

2. Experimental

Fig. 1 shows a schematic diagram of the experimental set-up for the laser induced etching. A commercially available n-type Si wafer with resistivity of 1 Ohm-cm was immersed in hydrofluoric acid with 49% concentration placed in a Teflon container and was supported on two Teflon plates. Laser etching was done by using an argon–ion laser with photon energy of 2.54 eV (λ= 488 nm). The beam was focused to a circular spot of 1.5mm diameter with a power density of 12 W cm^{-2}. The samples were etched in this way for 30, 60 and 90 min of exposure with the laser and subsequently the samples were rinsed with ethanol and dried with filtered N_2. The surface morphology of the etched PS was studied by SEM.

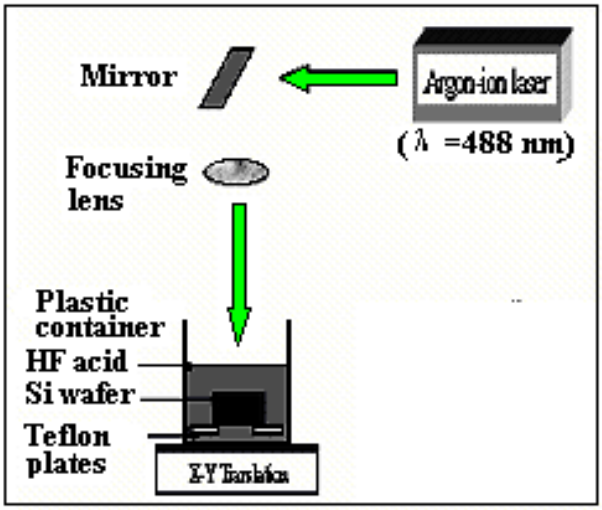

Fig. 1. The experimental set up of the laser-induced etching.

3. Results and discussion

3.1 Surface morphology and Laser-Induced Etching mechanism

In laser-induced etching, when n-type Si wafers are immersed in aqueous HF acid and illuminated with laser light, the photon energy will be absorbed by electrons in the valence band and excited to the conduction band, that will result into photogeneration of electron hole pairs as [11]

$$N_p = \frac{P}{h\nu}, \tag{1}$$

where N_p is the number of photons irradiated on silicon wafer per unit time, P is the power of the laser, $h\nu$ is the energy of the photon, and ν is the frequency of the laser. Then the number of electron-hole pairs generated is

$$G = \eta N_p \tag{2}$$

where η is the quantum coefficient of Si.

Given that, the sample is an n-type silicon wafer, holes will be generated on the polished surface and a depletion layer will form in the silicon wafer such that the polished surface is relatively positive in charge while the back side of the wafer is negative. This created a net flow of charges from the negative to the positive side, resulting in a current flow which will be completed by ions flowing in the HF aqueous solution. This net perpendicular flow of charges across the wafer will encourage the etching in the direction normal to the surface, which result in the formation of porous layer at the top of the silicon wafer. The porous layer thickness depends on the etching time, due to the fact that the number of photons irradiated on the sample increased with time.

Fig. 2 shows the SEM image of the etched Si wafer prepared by laser-induced etching using an argon–ion laser in the HF etching solution. At the top surface, microcrystallites of micrometer size with pits were observed. The thickness of the etched layer is about 3 μm and is quite uniform. The SEM micrograph shows microstructures of size ~5 μm. It was found that surfaces etch pits were formed on the surfaces of all irradiated area. The etch pits sizes range from 3 to 5 μm and they are strongly dependent on the etching conditions. The HF concentration has no significant effect on the density of the etch pits. However, with increasing etching time Fig. 2, (b and c) the total number of etches pits increases and their sizes become smaller.

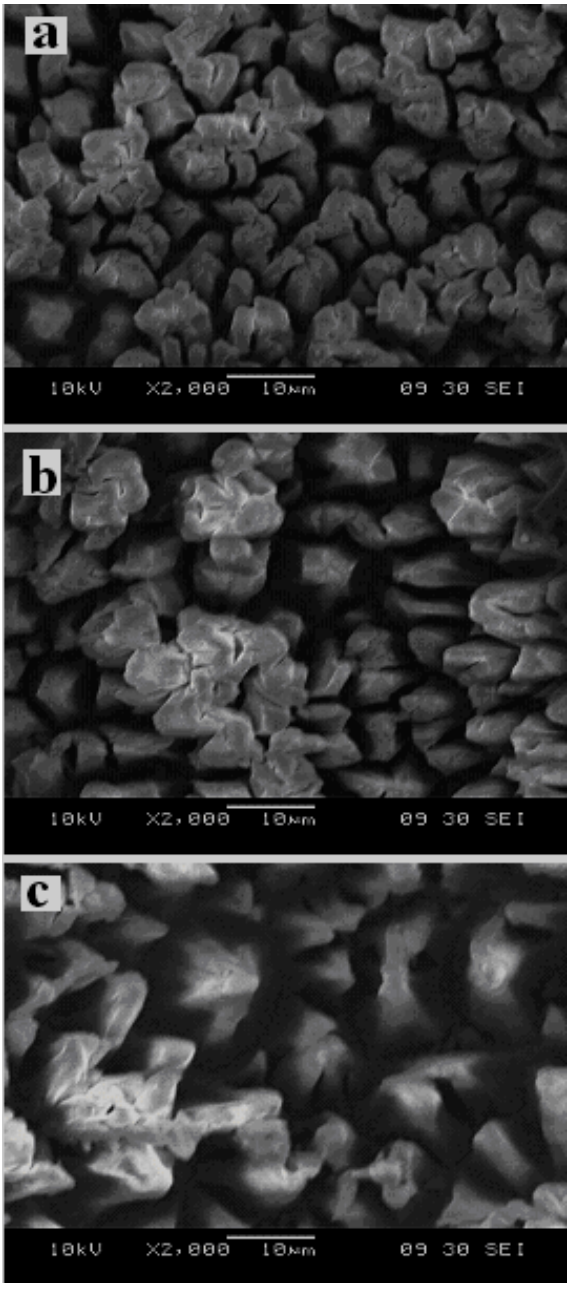

Fig. 2. SEM images of PS samples etched with different time, for (a) 30 min, (b) 60 min and (c) 90 min.

3.2 Raman spectroscopy

Raman spectroscopy provides a rapid, nondestructive, and simple diagnostic method for determining the nanocrystal dimensions. Basically, confinement of the electrons and phonons in reduced dimensional systems lead to major modifications in their electronic and vibrational properties. The vibrational modes, observed in the Raman spectra, are sensitive to the sizes. Different sizes of nanocrystallites will affect the shift, broadening, and lineshape of the Raman signal in different ways.

Fig. 3, shows typical Raman spectra of our PS samples (a, b, and c) prepared with different time of 30, 60, and 90 min. respectively. The spectrum from a crystalline silicon (c-Si) wafer is also shown for comparison. The peak position and width of sample (a) only have small changes compared to those of (c-Si) and other samples (b, and c). For the etching time of 60 min, the Raman line peak position shifts to a lower frequency of 518 cm^{-1} after etching. Furthermore, the Raman line is wide and asymmetric in comparison to the Raman line from (c-Si) for which the line has a narrow and symmetric shape centered at 521 cm^{-1}. The lineshape asymmetry increases as the etching time increases, and there exists a large peak shift from 521 cm^{-1} (c-Si) to 513 cm^{-1} (sample (c)) and a broadening of peak width and FWHM from 3 cm^{-1} (symmetric) to 8 cm^{-1} (asymmetric). Raman peak positions for samples (a), (b) and (c) are 519.6 cm^{-1}, 518.4 cm^{-1} and 516.9 cm^{-1}, respectively.

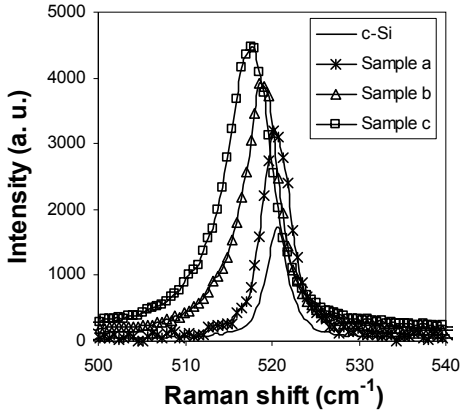

Fig. 3. Raman spectra of PS samples; a, b, and c, compared to unetched c-Si.

A theoretical fit to the experimental curve is obtained by using the three-dimensional quantum confinement model incorporating size distribution. To explain our experimental results in Fig. 3, a theoretical fit to the experimental curve is obtained by using the three-dimensional quantum confinement model incorporating size distribution. A quantitative model was developed by [14] and was later improved by [15]. This model was employed to estimate the average size or correlation length L of the nanocrystals from the Raman spectrum. The PS is modeled as an assembly of quantum dots, i.e. the confinement is three dimensional. For spherical nanocrystallites, the first order Raman line shape for longitudinal optical mode *LO* phonon is given by [15]

$$I_{LO}(\omega) = \int_0^1 \frac{4\pi q^2 \left|c(0,q)\right|^2}{\left[\omega - \omega_{LO}(q)\right]^2 + \left[0.5\ \Gamma_c\right]^2}\, d^3q \qquad (3)$$

$$\text{where} \quad \left|c(0,q)\right|^2 = \exp\left(\frac{-q^2 L^2}{4a^2}\right)$$

and the wave vector q is expressed in the units of $2\pi/a$ (a = c-Si lattice constant, 0.54 nm), L is the diameter of the Si nanocrystallite, ω_{LO} is the longitudinal phonon frequency at q along <100> direction and Γ_c is the FWHM of the crystalline silicon (3 cm^{-1}). The phonon dispersion relation $\omega_{LO}(q)$ according to [11] is

$$\omega_{LO}^2(q) = A + B\cos(\pi q/2), \qquad (4)$$

where, $A = 1.7207$ x 10^5 cm^{-2} and $B = 1.0$ x 10^5 cm^{-2}.

Equation (4) gives $\omega_{LO}(q = 0)$ as 521.6 cm^{-1}. The size estimated from equation (3), after etching process are 3.4, 3, and 2.2 nm for samples a, b, and c, respectively.

3.3 Photoluminescence spectra

The PL spectra of the as-prepared samples are presented in Fig. 5. As seen from the figure the samples show a PL band at ~600 nm. The band intensity increases when the etching time increases combined with a slight blue shift as exhibited by sample (b). For longer etching time, there would be a larger etched surface to emit light. Apart from this, the porous layer will also extend into the bulk; the irradiated region will therefore enlarge. Therefore, the PL intensity will increase. The changes in the PL intensity and peak position for the samples are in accordance with the observation, made in earlier studies [16, 17], such that the optical PL efficiency is high for smaller particles which emit at a shorter wavelength (higher energy).

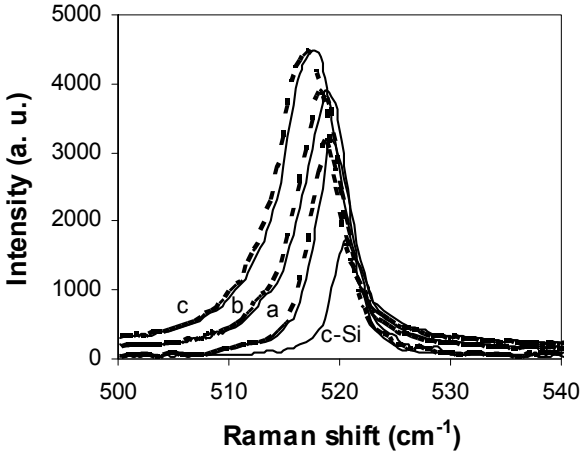

Fig. 4. Raman spectra of c-Si and PS samples; a, b, and c. The solid lines are the experimental data and the symbols are the generated spectra using the quantum confinement model.

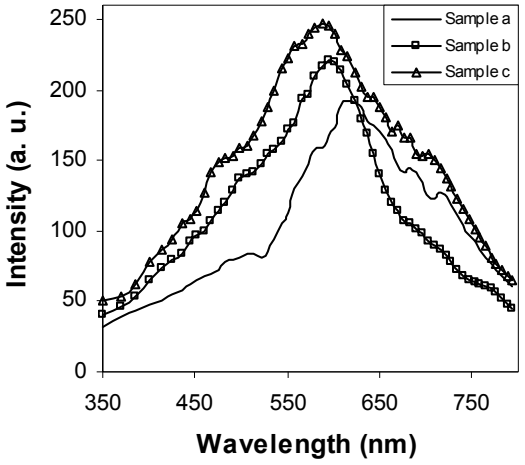

Fig. 5. The PL spectra of PS samples; a, b, and c, etched at different time.

To estimate the possible size of Si nanocrystals, we have used the equation describing a change of the band gap Δ E caused by the quantum confinement of charge carries in the effective mass approximation [18, 19]

$$E_g(L) = E_g(\infty) + \frac{\hbar^2 \pi^2}{2 L^2}\left(\frac{1}{m_e} + \frac{1}{m_h}\right) - \frac{1.786 e^2}{\varepsilon_r L} + 0.284 E^*_{Ry} \quad (5)$$

where $E_g(\infty)$ is the band gap of bulk Si, E^*_{Ry} the effective Rydberg energy, m_e and m_h are the effective masses of electron and hole, respectively, ε_r is the dielectric constant and e^2 =1.44 eV nm are taken from [3, 4]. Therefore, we can estimate that the observed PL peak at 622.7 nm (sample a) was due to Si nanocrystals of the radius of about 4.6 nm, and the observed PL peak at ~600 nm (samples b and c) was due to Si nanocrystals of ~4 nm. It should be noted that the PL measurement used 325 nm laser sources, while Raman measurement used 514.5 nm sources. Therefore any discrepancies between the information obtained from Raman and PL spectra could be attributed to the different penetration depths of the two techniques.

4. Conclusions

In summary, PS has been formed by laser-induced etching of n-type silicon. There is a reconstruction of the silicon surface and the changes in the surface morphology could be seen in the SEM investigations. The Raman spectra were also analysed using a three-dimensional confinement model. The red shift in the LO phonon Raman spectra and the blue shift in PL spectra reveal the quantum confinement effect in the Si nanocrystallites of the PS sample. As the etching time increases, these shifts increase due to decrease in the silicon nanocrystallite size. This is indicated by the decrease in the estimated diameter of spherical nanocrystallites from 3.4 to 2.2 nm using the Raman spectra.

Acknowledgment

The authors are grateful to School of Physics, Universiti Sains Malaysia, 11800 Penang, Malaysia for supporting this work under the project No. 304/PFIZIK/637040.

References

[1] L. T. Canham, Appl. Phys. Lett. **57**, 1046 (1990).
[2] P. Photopoulos and A. G. Nassiopoulou, J. Phys. Condens. Matter. **15**, 3641 (2003).
[3] H. S. Chen, J. J. Chiu, T. P. Perng. Mater. Phys. Mech. **4**, 62 (2001).
[4] L. T. Canham, W. Y. Leong, T. I. Cox, L. Taylor. Appl. Phys. Lett. **21**, 2563 (1992).
[5] H. D. Fuchs, M. Stutzmann, M. S. Brandt, M. Rosenbauer, J. Weber, A. Breitschwerdt, P. Deak, M. Cardona. Phys. Rev. B **48**, 8172 (1993).
[6] Cullis, L. T. Canham, P. D. J. Calcott. J. Appl. Phys, **82**, 909 (1997).
[7] Z. Gaburro, H. You, D. Babie. J. Appl. Phys. **84**, 6345 (1998).
[8] J. Sarathy, S. Shih, K. H. Jung, C. Tasi, K. H. Li, D. L. Kwong, J. C. Campbell. Appl. Phys. Lett. **60**, 1533 (1992).
[9] Y. Harada, X. Li, P. W. Bohn, R. G. Nuzzo. J Am Chem Soc, **123**, 8709 (2001).
[10] S. Chattopadhyay, X. Li, P. W. Bohn. J Appl Phys. **91**, 6134 (2002).
[11] C. H. Choy, K. W. Cheah. Appl. Phys. A, **61**, 45 (1995).
[12] H. S. Mavi, B. G. Rasheed, A. K. Shukla, S. C. Abbi K. P. Jain. J. Phys. D: Appl. Phys. **34**, 292 (2001).
[13] H. S. Mavi, B. G. Rasheed, R. K. Soni, S. C. Abbi, K.P. Jain. Thin Solid Films. **397**, 125 (2001).
[14] H. Richter, Z. P. Wang, L. Ley, Solid State Commun. **39**, 625 (1986).
[15] H. Campbell, P. M. Fauchet, Solid State Communications, **58**, 739 (1986).
[16] R. Tsu, H. Shen, M. Dutta Appl. Phys. Lett. **60**, 112 (1992).
[17] N. A. Hill, K. B. Whaley Phys. Rev. Lett. **75**, 1130 (1995).
[18] Brus JE. J Lumin 31,381 (1984).
[19] Kayanuma Y. Phys Rev B**38**, 9797 (1988).
[20] Sze S M. Physics of semiconductor Devices.John Wiley and Sons Inc New York; 1981
[21] Wolf S, Tauber R. Silicon Processing for the VLSI Era. Lattice Press Sunset Beach California; 1986.

*Corresponding author: khalhadithi@yahoo.com